The Plant Cell, Vol. 17, 1167–1179, April 2005, www.plantcell.org

Structural Basis of Eukaryotic Nitrate Reduction: Crystal Structures of the Nitrate Reductase Active Site

Katrin Fischer,[a] Guillaume G. Barbier,[b,c] Hans-Juergen Hecht,[d] Ralf R. Mendel,[a] Wilbur H. Campbell,[b,c] and Guenter Schwarz[a,1]

[a] Institute of Plant Biology, Technical University Braunschweig, D-38106 Braunschweig, Germany
[b] Nitrate Elimination Company, Lake Linden, Michigan 49945
[c] Department of Biological Sciences, Michigan Technological University, Houghton, Michigan 49931
[d] German Research Center for Biotechnology, D-38124 Braunschweig, Germany

Nitrate assimilation in autotrophs provides most of the reduced nitrogen on earth. In eukaryotes, reduction of nitrate to nitrite is catalyzed by the molybdenum-containing NAD(P)H:nitrate reductase (NR; EC 1.7.1.1-3). In addition to the molybdenum center, NR contains iron-heme and flavin adenine dinucleotide as redox cofactors involved in an internal electron transport chain from NAD(P)H to nitrate. Recombinant, catalytically active *Pichia angusta* nitrate-reducing, molybdenum-containing fragment (NR-Mo) was expressed in *P. pastoris* and purified. Crystal structures for NR-Mo were determined at 1.7 and 2.6 Å. These structures revealed a unique slot for binding nitrate in the active site and identified key Arg and Trp residues potentially involved in nitrate binding. Dimeric NR-Mo is similar in overall structure to sulfite oxidases, with significant differences in the active site. Sulfate bound in the active site caused conformational changes, as compared with the unbound enzyme. Four ordered water molecules located in close proximity to Mo define a nitrate binding site, a penta-coordinated reaction intermediate, and product release. Because yeast NAD(P)H:NR is representative of the family of eukaryotic NR, we propose a general mechanism for nitrate reduction catalysis.

INTRODUCTION

Assimilatory NAD(P)H:nitrate reductases (NR; EC 1.7.1.1-3) catalyze the first and rate-limiting steps of nitrate assimilation in plants, algae, and fungi (Campbell, 2001). NR belongs to the molybdenum cofactor (Moco)–containing family of enzymes that catalyze two-electron transfer reactions in global C, N, and S cycles (Hille, 1996). These processes include nitrate reduction, abscisic acid biosynthesis, purine catabolism, and sulfite detoxification in plants and sulfite detoxification and purine catabolism in mammals (Mendel and Schwarz, 1999). All eukaryotic molybdenum enzymes share a common molybdenum (Mo) atom that is bound to two sulfur atoms (ene-dithiolate) of a pyranopterin derivative, called molybdopterin. The structural core of this molybdopterin is conserved among all kingdoms and is found in all Mo-containing enzymes, except nitrogenase.

Eukaryotic NR is only active as a homodimer, and dimerization is dependent on the presence of Moco (Campbell, 2001). The NR monomer contains three distinguishable sequence regions associated with the Mo center, the Fe-heme of the cytochrome b_5 domain, and a C-terminal domain associated with a flavin adenine nucleotide (FAD) cofactor (Figure 1A). NR dimerization is mediated by the Mo-containing fragment, which can be further subdivided into the N-terminal Moco binding and C-terminal dimerization domains. The latter was identified in the crystal structure of the homologous sulfite oxidase (SO). The cytochrome b_5 domain is separated from the dimerization domain by a solvent-exposed linker region, named hinge 1, whereas the linker between the cytochrome domain and the FAD domain is referred to as hinge 2 (Figure 1A). In plants, hinge 1 bears a regulatory Ser residue that upon phosphorylation mediates the inhibition of NR by a 14-3-3 protein (Kaiser and Huber, 2001; MacKintosh and Meek, 2001). The Moco domain is preceded by an N-terminal extension rich in acidic residues that varies between 7 and 121 residues in length in fungi and 60 to 99 residues in plants without any significant conservation. A possible role of this extension in plants is seen in posttranscriptional regulation (Nussaume et al., 1995).

NR occurs in three different forms: NADH-specific forms are frequently present in higher plants and algae, NADPH-specific forms are unique in fungi, and NAD(P)H-bispecific forms are found in all aforementioned organisms, being most common in fungi (Campbell and Kinghorn, 1990). The catalytic cycle of NR can be divided into three parts: a reductive half-reaction in which NAD(P)H reduces FAD, electron transfer via the intermediate cytochrome b_5 domain, and an oxidative half-reaction in which the Mo center transfers its electrons onto nitrate, thereby forming nitrite and hydroxide (Skipper et al., 2001). The rates of intramolecular electron transfer between the domains in *Arabidopsis thaliana* NR are similar. Therefore, it seems that none of the steps are rate limiting (Skipper et al., 2001). Several fragments of

[1] To whom correspondence should be addressed. E-mail g.schwarz@tu-bs.de; fax 49-531-391-8208.
The author responsible for distribution of materials integral to the findings presented in this article in accordance with the policy described in the Instructions for Authors (www.plantcell.org) is: Guenter Schwarz (g.schwarz@tu-bs.de).
Article, publication date, and citation information can be found at www.plantcell.org/cgi/doi/10.1105/tpc.104.029694.

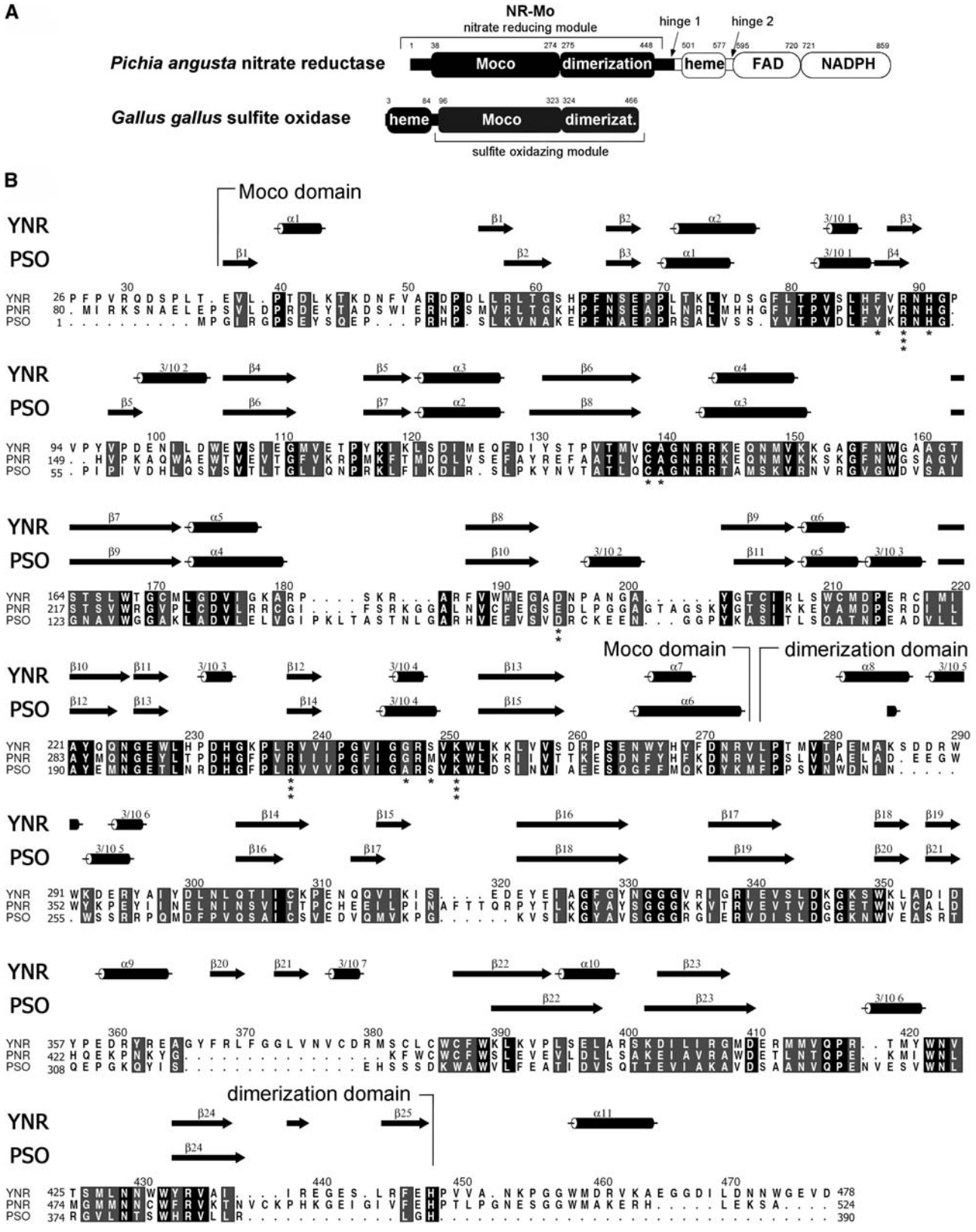

Figure 1. Primary and Secondary Structure Comparison of NR and SO.

NR have been recombinantly expressed, each of which possesses partial catalytic activity or characteristic spectral properties of the holoenzyme (Lu et al., 1992; Ratnam et al., 1997; Pollock et al., 2002). Analysis of a fragment containing heme and FAD domains of spinach (*Spinacia oleracea*) NR indicated that electron transfer from heme appeared to be slightly slower than FAD reduction (Ratnam et al., 1997). For the spinach NR Mo domain, nitrate K_m is 8 to 12 μM (Pollock et al., 2002); whereas for the corresponding nitrate-reducing fragment from yeast NR, the nitrate K_m is 30 μM (Barbier et al., 2004).

The primary structure of NR is conserved among plants, algae, and fungi, whereas they are completely different from bacterial NR regarding sequence similarity and structural composition. The latter belong to the dimethyl sulfoxide reductase family of Mo enzymes, and they contain a different type of Moco as well as iron-sulfur clusters as additional prosthetic groups (Stolz and Basu, 2002). Eukaryotic NR belongs to the SO family of Mo enzymes for which the first crystal structure was determined for chicken SO (CSO) (Kisker et al., 1997). Recently, the structure of Arabidopsis SO (plant SO [PSO]), a plant homolog of animal SOs, has been determined and provided additional insights into animal and plant sulfite oxidation (Schrader et al., 2003). PSO is the simplest Mo enzyme known so far that possesses a single catalytically active center, the Moco domain (Eilers et al., 2001). For eukaryotic NR, only the individual structure of the maize (*Zea mays*) FAD domain (Lu et al., 1994, 1995) has been determined so far.

To investigate the structure and function of eukaryotic NR, we have expressed and purified the Mo-containing nitrate-reducing N-terminal fragment (residues 1 to 484) of yeast NAD(P)H:NR (NR-Mo) from *Pichia angusta*, using *P. pastoris* as host. We have determined two crystal structures of NR-Mo at 1.7- and 2.6-Å resolution. These structures provide essential and novel information on the nitrate-reducing active site of eukaryotic NR and assist with identification of key active site residues involved in nitrate binding and other facets of the catalytic mechanism. The overall fold of the dimeric NR-Mo is similar to SO forms, though differences occur in the N- and C-terminal parts, and in an additional loop, as well as near the active site. In the 1.7-Å structure, a bound sulfate caused several conformational changes in the active site as compared with unbound NR-Mo, and four ordered water molecules were found in close proximity to Mo. Based on these water molecules, we defined a mechanism for nitrate reduction catalyzed by NR involving nitrate binding, formation of a penta-coordinated reaction intermediate, and formation of the products, nitrite and water.

RESULTS AND DISCUSSION

Structure Determination

The crystal structure of NR-Mo was determined by molecular replacement using a monomer of PSO (Protein Data Bank entry 1OGP) (Schrader et al., 2003) as search model. First, the 2.6-Å data set (NR-Mo1) was refined to a final R-factor of 18.4% (R_{free} = 24.9%) and subsequently used to determine the structure of the high-resolution 1.7-Å data set of NR-Mo2, which was refined to an R-factor of 16.7% (R_{free} = 19.5%). Both models have excellent stereochemistry (Table 1). The NR-Mo1 model contains one monomer with residues 26 to 478, one Moco, and 59 water molecules in the asymmetric unit. NR-Mo2 comprises two monomers in the asymmetric unit, each defined by residues 64 to 478, and 799 water molecules. In addition to the Moco, one Na^+ ion, two sulfate ions, and two glycerol molecules were bound per monomer in NR-Mo2 and were derived from the crystallization buffer as well as the cryoprotectant. Except for both termini, all atoms are well defined in both NR-Mo models. The first 25 residues in NR-Mo1 and the first 63 residues in NR-Mo2 are disordered or degraded, respectively, as well as the last six residues (479 to 484) in both crystal forms.

Fold of the Monomer

The NR-Mo monomer is characterized by a slightly elongated shape and a mixed α+β structure similar to the SO fold (Kisker et al., 1997; Schrader et al., 2003) (Figures 1 and 2) and is clearly divided into two domains (Figure 2A). The N-terminal Moco binding domain (residues 38 to 274) comprises 13 β-strands, organized in one mixed and two antiparallel β-sheets as well as seven α-helices and four 3_{10}-helices. An N-terminal three-stranded antiparallel β-sheet is formed (β1-β3) that leads into a five-stranded mixed β-sheet (β4, β5, β8, β9, and β13) located on the opposite site of the domain. The central motif of this domain, a five-stranded antiparallel β-sheet (β6, β7, and β10 to β12), is separated from the mixed β-sheet by nine short helices (α1, α3, α5 to α7, and 3_{10}1 to 3_{10}4). Between the two longest β-strands of this domain (β6 and β7), a long hairpin loop with a short helix (α4) is inserted, which is responsible for hydrophobic and polar interactions with the C-terminal domain. The core of the C-terminal dimerization domain (residues 275 to 448) constitutes as main feature a Greek key motif that is formed by two large antiparallel β-sheets. The first sheet contains four strands (β14, β16, β19, and β22), whereas the other sheet consists of

Figure 1. (continued).

(A) Domain structure of *P. angusta* NR and CSO. The NR-Mo fragment that has been expressed, purified, and crystallized is shown in black. The first and last residues of conserved domains (Moco binding, dimerization, heme, FAD, and NADPH binding domains) are indicated.

(B) Sequence alignment of yeast NR (*P. angusta*, YNR) and Arabidopsis NR2 (plant NR, PNR) with Arabidopsis SO (plant SO, PSO). Strictly conserved residues are highlighted in black, and conserved residues are highlighted in gray. Secondary structure elements for YNR and PSO are shown above the alignment with cylinders for α- or 3_{10}-helices and arrows for β-sheets. The alignment was generated with ClustalW (Thompson et al., 1994) and ALSCRIPT (Barton, 1993). Secondary structure elements were determined with PROMOTIF (Hutchinson and Thornton, 1996). Residue numbering is based on the primary sequence of YNR. Residues of NR-Mo that coordinate the Moco are indicated with asterisks. The number of asterisks correlates with the number of contacts to Moco.

Table 1. Data Collection and Refinement Statistics

Data Set	NR-Mo1	NR-Mo2
Data collection		
Wavelength (Å)	1.005	1.005
Space group	$P6_122$	$C222_1$
Unit cell dimensions a, b, and c (Å)	76.7, 76.7, and 306.1	122.7, 123.0, and 149.5
Resolution limits (Å)	30–2.6	25–1.7
Completeness (%)	99.6	99.0
R_{sym} (last shell)[a]	0.088 (0.438)	0.093 (0.445)
I/sigI (last shell)[b]	24.7 (3.3)	4.6 (1.6)
Refinement statistics		
Number of observed reflections	139508	2235039
Number of unique reflections	17438	123668
Number of residues	A26–A478	A64–A478 and B64–B478
Number of ions	–	4 sulfate, 2 natrium
Number of solvent molecules	59 water	799 water, 6 glycerol
R_{cryst} (R_{free})[c]	0.184 (0.249)	0.167 (0.195)
Deviations from ideal values		
Bond distances (Å)	0.017	0.016
Angle distances (°)	1.575	1.544
Torsion angles (°)	7.322	6.101
Chiral-center restraints (Å^3)	0.092	0.205
Planar groups (Å)	0.006	0.008
Ramachandran statistics[d]	0.873/0.125/0.3/0	0.913/0.087/0/0

[a] $R_{sym} = \Sigma_{hkl}\Sigma_i|I_i - \langle I\rangle|\Sigma_{hkl}\Sigma_i\langle I\rangle$, where I_i is the ith measurement, and $\langle I\rangle$ is the weighted mean of all measurements of I.

[b] $\langle I\rangle/\langle\sigma I\rangle$ indicates the average of the intensity divided by its average standard deviation.

[c] $R_{cryst} = \Sigma||F_o| - |F_c||/\Sigma|F_o|$, where F_o and F_c are the observed and calculated structure factor amplitudes. R_{free} same as R_{cryst} for 5% of the data randomly omitted from the refinement.

[d] Ramachandran statistics indicate the fraction of residues in the most favored, additionally allowed, generously allowed, and disallowed regions of the Ramachandran diagram, as defined by PROCHECK (Laskowski et al., 1993).

six strands (β15, β17, β18, and β23 to β25). A third antiparallel β-sheet composed of two short strands (β20 and β21) forms together with two helices (α9 and $3_{10}7$) an extension located in proximity to the central motif of the Moco domain. The N-terminal part of the dimerization domain comprises three helices (α8, $3_{10}5$, and $3_{10}6$) that are organized in an extended loop. At the C terminus of NR-Mo, the linker leading into the cytochrome b_5 domain of NR contains one helix (α11). The dimerization domain possesses a similar topology to the C2 subtype immunoglobulin superfamily (Vaughn and Bjorkman, 1996) as described for the corresponding domain of SO (Kisker et al., 1997).

In contrast with the available databank entries for *P. angusta* NR-Mo, no electron density was found for the side chain of residue 203 in both structures resulting in the substitution of Arg for Gly. Three *cis*-peptides were found in both models (His63-Pro64, Lys235-Pro236, and Lys309-Pro310) for which two or three homologous *cis*-peptides were also found in PSO (Glu26-Pro27 and Phe204-Pro205) and CSO (Lys113-Pro114, Phe285-Pro286, and Gln353-Pro354), respectively (Kisker et al., 1997; Schrader et al., 2003). In the high-resolution NR-Mo2 structure, one Na^+ ion and two sulfate molecules are bound at identical sites in each monomer. The Na^+ is bound via hydrogen bonds to both monomers via the main chain carbonyl of Asp410 (2.86 Å) and Arg339Nε (3.22 Å) in one monomer and the main chain carbonyl of Arg295 (2.86 Å) of the dimerization domain in the other monomer. One sulfate molecule is in close proximity to the Moco in the wider part of the substrate funnel and forms contacts with Asn66, Arg89, and Phe156 via four hydrogen bonds (see below). The second sulfate molecule is located in a remote position only bound by Lys145Nξ (α4).

Both NR-Mo2 monomers are very similar, as indicated by an overall root mean square (rms) deviation of 0.045 Å for all 415 residues. When comparing the monomers of both crystal forms (Figure 2B), an rms deviation of 0.505 Å is observed, caused by the differently orientated termini, some minor changes in loop regions (Figure 2B, arrows), and conformational changes close to the active site-bound sulfate, which will be discussed below.

Fold of the Dimer

In both crystal forms, the asymmetric unit is formed by individual NR-Mo monomers. However, in both cases, dimers are formed along twofold crystallographic symmetry axes. The dimerization is consistent with earlier studies (Campbell and Kinghorn, 1990) on the structure and function of eukaryotic NR, and it was used as a quality criterion to evaluate the molecular replacement solution during structure determination. Because these dimers are nearly identical and tightly associated in both crystal forms, dimerization is the native oligomeric state of NR-Mo. The crystallographic dimers in both NR-Mo structures (Figure 2C)

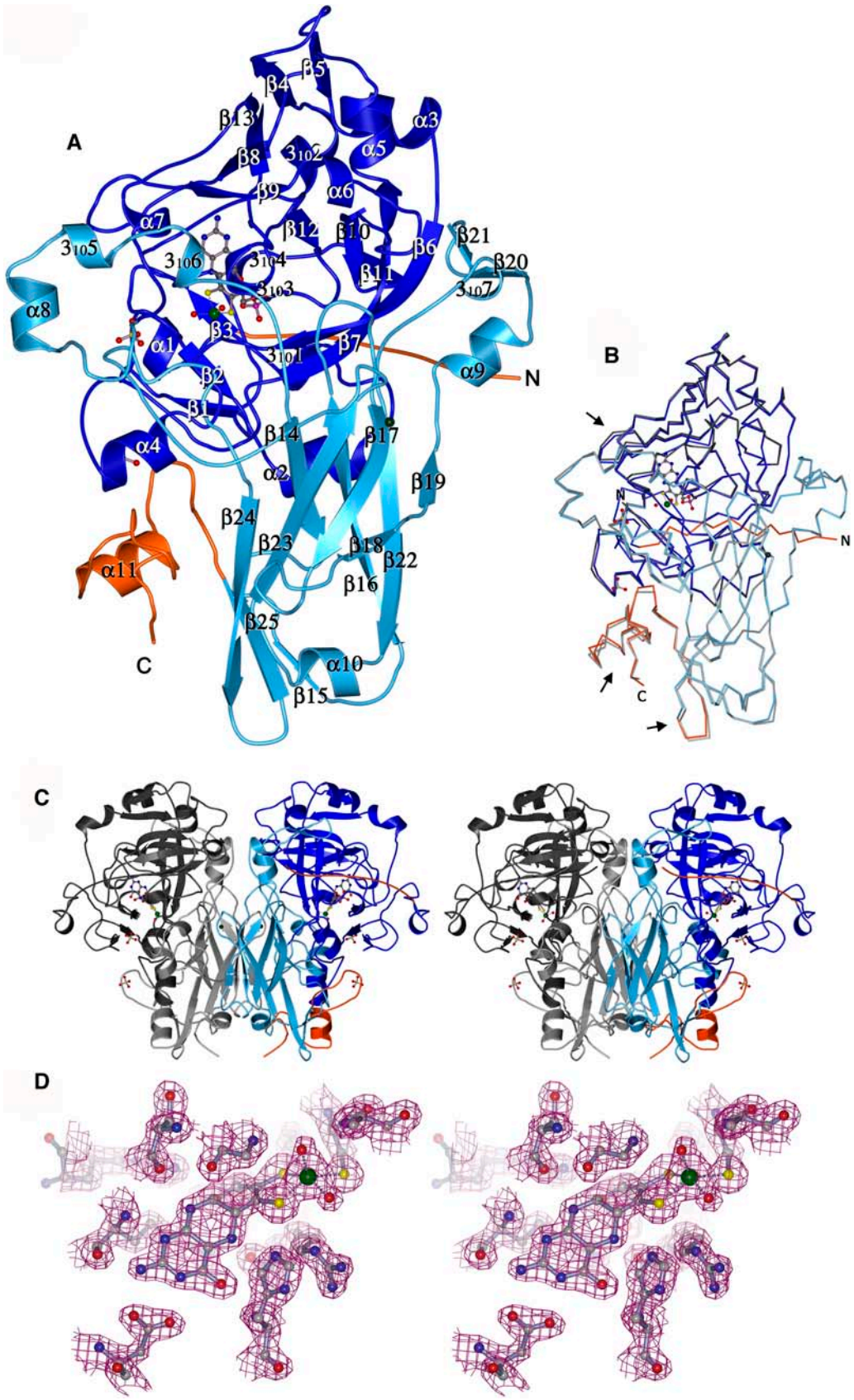

Figure 2. Overall Structure of NR-Mo.

have overall dimensions of 98 × 79 × 75 Å^3, and the dimer interface extends over 2190 Å^2, corresponding to 12% of the accessible surface area of each subunit. Dimerization is mainly mediated by the C-terminal domain with some additional interactions between the Moco domains. In both structures, the dimers are stabilized by 39% polar and 61% nonpolar interface residues. The average predicted number of 1.0 hydrogen bond per 75 Å^2 of polar dimer interface (Bahadur et al., 2004) is well exceeded in both crystal structures with 1.6 and 2.0 hydrogen bonds per 75 Å^2 of hydrophilic interface in NR-Mo1 and NR-Mo2, respectively. Disulfide bridges were not found in any of the two crystal forms of NR-Mo. In total, 36 hydrogen bonds and salt bridges are responsible for direct intersubunit contacts in NR-Mo1, whereas in NR-Mo2, 44 direct intersubunit bonds are found. These extra bonds might be one reason for the high-resolution diffraction of NR-Mo2.

Comparison of NR-Mo and SOs

On the level of primary amino acid sequence, the *P. angusta* NR-Mo shares 38% identity with Arabidopsis NR-Mo, 26% with PSO, and 27% with the CSO Mo domain. The conservation of the Moco binding domains is significantly higher, accompanied by less conservation of the dimerization domains (Table 2). These homologies are consistent with the observed rms deviations among the structures of NR-Mo, PSO, and CSO (Table 2). The overall topology of the Mo domain monomers adopts a very similar fold in all three proteins (Figure 4A). NR-Mo exhibits one additional feature, which is unique among all fungal NRs (Figures 1B and 2B) due to an insertion of 14 to 16 residues forming α9, β20-β21, and 3_{10}7. More differences exist at both termini and in another loop region (α8, 3_{10}5 and 3_{10}6) near the active site, which replaces the single helix (3_{10}2) of PSO. The N-terminal region of NR-Mo preceding the Moco domain has a unique fold clinging to the core of the Moco domain, whereas in CSO, the N terminus of the Moco domain is attached to the cytochrome b_5 domain, thus adopting a different orientation, and PSO completely lacks such an N-terminal extension (Figure 1A). The C terminus is also arranged differently in all three proteins. SO structures terminate within a few residues after the dimerization domain, whereas the C terminus of the NR-Mo dimerization domain bears an additional β-strand (β25) and then continues with the linker toward the cytochrome b_5 domain. This extension mainly contributes to the somewhat larger dimerization domain of NR-Mo (Figure 1A). In NR-Mo, the C terminus is clearly separated from the dimerization domain and therefore surface exposed, a fact that explains the protease sensitivity of the hinge 1 region connecting the dimerization domain with the cytochrome b_5 domain. Solvent exposure is also key to phosphorylation of the regulatory Ser in hinge 1 of plant NR forms and the subsequent binding of the inhibitory 14-3-3 protein (Kaiser and Huber, 2001; MacKintosh and Meek, 2001).

The Moco Domain

Both models show well-defined electron density for the Moco, in particular, in the high-resolution 1.7-Å structure, all Moco atoms, including both terminal oxygens, are covered by electron density, indicating high cofactor saturation (Figure 2D). Moco is composed of a single molybdopterin (pyranopterin) and deeply buried in the Moco domain forming 14 hydrogen bonds to main chain and side chain atoms of Moco domain residues (Figure 3). All cofactor binding residues are highly conserved among NRs and SOs (data not shown). In both monomers of NR-Mo2, the Mo is coordinated by five ligands forming an almost perfect square pyramidal geometry (Figure 2D). Two sulfur atoms originating from molybdopterin, one sulfur from the conserved Cys139 as protein ligand, and one oxygen ligand (O6) occupy the equatorial plane, whereas the axial position is assigned to another oxygen atom (O5). This axial oxygen ligand is stabilized by two hydrogen bonds to the terminal amino groups of Ala140 and Gly247 (Figure 3) that are also conserved in CSO (Figure 1B) (Kisker et al., 1997).

The dioxo Mo center, which is a common feature of the SO family (Hille, 1996), could be assigned to a Mo(IV) state, with similar Mo-O distances to the CSO structure, with 1.7 Å for the apical oxygen and 2.3 Å for the equatorial hydroxo/water ligand (Kisker et al., 1997). In the oxidized state (MoVI), both Mo-oxo distances would be ~1.7 Å as proposed for animal SO (George et al., 1999). In NR-Mo2, when using an omit-map where Moco was excluded from the refinement, the center of electron density for the equatorial O6 was 2.41 to 2.46 Å away from Mo; whereas the Mo-O5 distances for the apical oxygen were estimated to be 1.75 to 1.80 Å because of interferences by the large electron density peak centered on the Mo atom. The reduced Mo in NR-Mo2 (MoIV) can be explained by the purification of NR-Mo under reducing conditions (see Methods) or photoreduction as probably occurred in CSO (Kisker et al., 1997).

Figure 2. (continued).

(A) Ribbon presentation of the NR-Mo monomer. The two domains are colored dark blue (Moco domain) and light blue (dimerization domain), and the nonconserved N-terminal part and the C-terminal linker region is colored orange. The Moco, Na^+, and sulfates are shown in ball-and-stick representation, β-strands as curved arrows, and α- and 3_{10}-helices as ribbons. The bonds between Mo and all five ligands are plotted as dashes (cf. **[D]**). The model is a composite of residues 26 to 70 from NR-Mo1 and residues 71 to 478 from NR-Mo2.

(B) Superposition of NR-Mo1 and NR-Mo2 monomers. NR-Mo1 is colored and orientated as in **(A)**; NR-Mo2 is shown in gray.

(C) Stereo view of the NR-Mo dimer in ribbon presentation (merged as in **[A]**). For one monomer, the color coding is the same as in **(A)**, and the second monomer is shown in dark and light gray.

(D) Stereo close-up view of Moco and coordinating residues shown in ball-and-stick representation, with dashed bonds between Mo and its five ligands. The $2F_o$-F_c electron density map is contoured at 1.0 σ. The figure was generated with MOLSCRIPT (Esnouf, 1997) and rendered with POVRAY (www.povray.org).

Table 2. Homologies and rms Deviations within Domains of Mo Enzymes of the SO Family

	PSO		CSO		PNR[b]	
NR-Mo1 (NR-Mo2)	rms Deviation	Identity[a]	rms Deviation	Identity	rms Deviation	Identity
Moco domain						
39–274 (64–274)	1.25 (1.14)	0.320	1.12 (1.07)	0.326	–	0.492
Dimerization domain						
275–448	1.31 (1.29)	0.227	1.41 (1.42)	0.227	–	0.305
Overall						
39–448	1.53 (1.52)	0.259	1.47 (1.53)	0.265	–	0.382

[a] Identities were calculated according to (Combet et al., 2000).
[b] PNR, plant NR from Arabidopsis.

Surface Properties

NR-Mo possesses positively charged residues surrounding the substrate funnel (Figure 4B, arrow). This positively charged cavity seems to be a common feature of both NRs and SOs as these enzymes act on anions. The charge distribution of NR-Mo is not as prominent as in PSO and CSO. Furthermore, there is a significant patch of negative charge right above the entrance to the active site that is unique to NR. Another important difference is the shape of the substrate binding cavity itself. In NR-Mo, the substrate funnel narrows to an elongated slot, which provides enough space for the planar nitrate molecule, but not for a bulky sulfate molecule (Figures 4B, 5C, and 5D). Therefore, it is not surprising that sulfate does not inhibit NR, whereas nitrate is an inhibitor of SO (Kessler and Rajagopalan, 1974). However, except for the negative patch above the active site entrance, all other surrounding surface residues are well conserved among all members of the SO family (Figures 4C and 4D). Surface residues that are only conserved in NRs are found right below and above the active site funnel (Figure 4C, light green patches). Some of the residues in the upper part (Figure 4C, dark green) are also conserved in animal SOs (but not in PSOs), and they belong to a region of the molecule that has been predicted to be important for binding the cytochrome b_5 domain (Schrader et al., 2003) and is therefore essential for effective intramolecular electron transfer. For animal SOs, a model for dynamic electron transfer from the Moco to the heme has been proposed where the cytochrome b_5 domain is moving in close proximity to the active site of the Mo domain (Feng et al., 2002). This model is based on the crystal structure (Kisker et al., 1997) and biochemical studies (Feng et al., 2002) that have demonstrated a reduced intramolecular electron transfer rate with increased solution viscosity.

The question remains open whether or not the mechanism of intramolecular electron transfer in NR might be similar to animal SO. For NR, it has been shown recently that increased solution viscosity also decreases nitrate-reducing catalytic activity (G.G. Barbier and W.H. Campbell, unpublished results). According to the domain structure of NR, the C-terminal linker between the Mo domain and the heme domain is solvent exposed in both NR-Mo structures. Similar to CSO, not all residues of the NR-Mo linker region are defined, which could either be due to the truncation of the protein or a general flexibility of the linker as in CSO. Clearly, the crystal structure of the holo-NR has to be determined to provide additional insights into the intramolecular electron transfer mechanism of NR.

The Active Site of NR and SO

Structural comparison between the active site of NR-Mo, PSO, and CSO (Figure 5A) revealed remarkable conservation on one side with Arg144, Trp158, and Arg89 (NR residues) perfectly

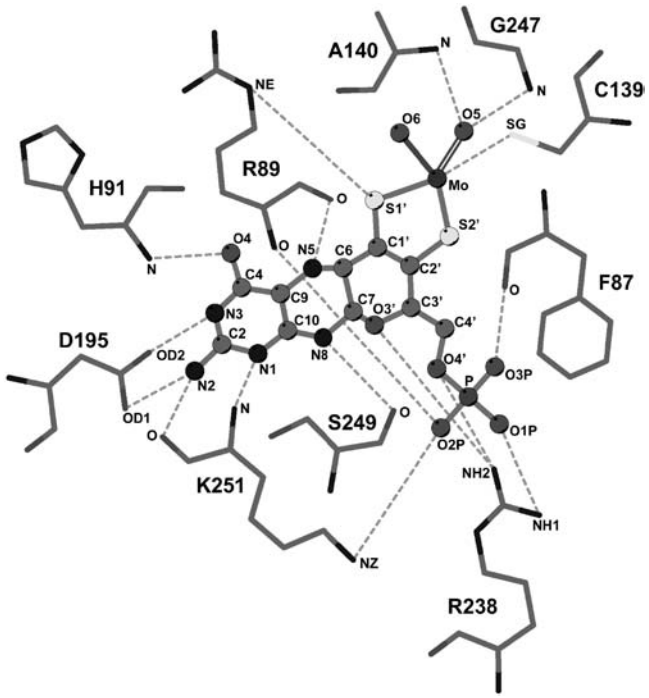

Figure 3. The Coordination of the Moco.

Schematic representation of all protein–Moco interactions. Hydrogen bonds are drawn as dashed lines. No water-mediated hydrogen bonds between the Moco and protein were observed. The hydroxy coordination of the equatorial Mo-bound oxygen (O6) is indicated by a bold solid line and the oxo-coordination of the apical oxygen (O5) by duplicate lines. Figure was generated with LIGPLOT (Wallace et al., 1995).

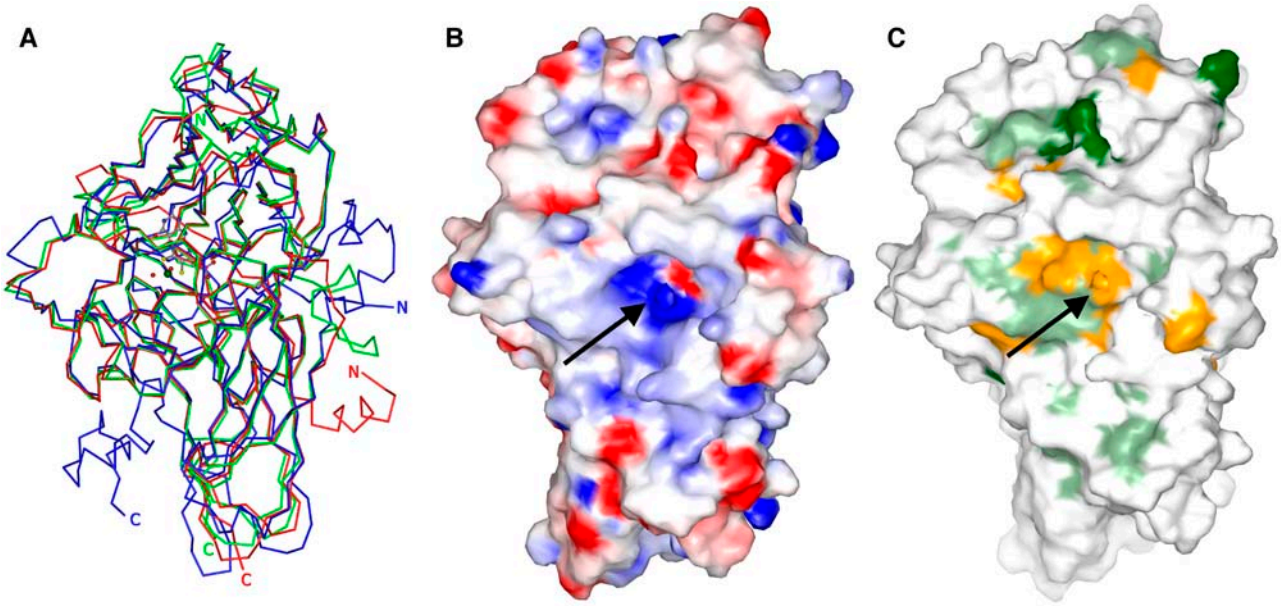

D

NR	*P.angusta*	RKEQNMVKKGAGFNWGAAGTSTSLW	168	VWMEGADN.PANGA.....YGT	204	YAIYDLNLQTIICKP	310	CWCFW	389
NR	*P.anomala*	RKEQNQVKKGKGFNWGAAGVSTSLW	170	VWMEGCDD.PAKGA.....YGT	206	YAIYDLNLQSITVYP	312	CWCFW	395
NR	*A.niger*	RKEQNVVRKTKGFSWGSAGLSTALW	182	VCMEGADKLPNGY......YGT	217	YAIYDLNVNSSVVYP	325	CWCFW	403
NR	*N.crassa*	RKEQNVLRKSKGFSWGAGGLSTALW	270	VCFEGADQLPNGT......YGT	310	YAIYDLNVNSVICEP	420	CWCFW	503
NR	*A.thaliana*	RKEQNMVKKSKGFNWGSAGVSTSVW	221	VCFEGSEDLPGGAGTAGSKYGT	265	YIINELNINSVITTP	371	CWCFW	437
NR	*N.tabacum*	RKEQNMVKQTIGFNWGAAAVSTTIW	213	VCFEGADVLPGGG...GSKYGT	254	YIINELNINSVITTP	360	CWCFW	426
NR	*H.vulgare*	RKEQNMVQQTVGFNWGAAGVSTSVW	216	VCFEGAEDLPGGG...GSKYGT	257	YIINELNTNSVITTP	363	CWCFW	429
SO	*G.gallus*	RSEMSRVRPVKGLPWDIGAISTARW	128	VCFEGLDADPGG.....APYGA	255	PAIQELPVQSAVTQP	268	AWALW	333
SO	*H.sapiens*	RSEMTQVKEVKGLEWRTGAISTARW	127	VCFEGLDSDPTG.....TAYGA	275	PSIQELPVQSAITEP	266	AWRLW	335
SO	*Drosopohila*	RSEMTKVKAVG.....NAKW	125	VIFEGADLDPTS.....HPYGA	354	DAIQAMPVTSAICTP	263	GWSLW	332
SO	*Arabidopsis*	RTAMSKVRNVRGVGWDVSAIGNAVW	128	VEFVSVDRCKEENG...GPYKA	173	RPQMDFPVQSAICSV	273	AWVLF	339
SO	*Oryza*	RTAMSKVRKVRGVGWDISALGNATW	128	VEFVSVDRCKEEKG...GPYKA	173	RPQMDFPVQSAICTL	273	AWVLF	339
SO	*Glycine*	RTAMSKTKTVKGVGWDVSAIGNAIW	128	VEFVSIDKCKEENG...GPYKA	173	.....		.....	
SO	*Triticum*	RTAMSKVRKVRGVGWDVSALGNATW	128	VEFVSVDRCKEEKG...GPYKA	173	.....		.....	

Figure 4. Comparisons between NR-Mo and SOs.

(A) Superposition of NR-Mo fragments from *P. angusta* NR (blue), PSO (green), and CSO (red). The figure was generated as described in Figure 2.
(B) Electrostatic surface potential of NR-Mo. Surface residues are color coded according to their charge (blue for positively charged and red for negatively charged side chains). Hydrophobic areas are not colored. The view is toward the entrance of the substrate funnel (arrow). The electrostatic potential map was calculated at an ionic strength of 100 mM and contoured at ± 10 k_BT (k_B, Boltzmann constant; T, absolute temperature).
(C) and **(D)** Conserved residues among enzymes of the SO family are shown on the surface **(C)** and in an alignment **(D)**. Residues that are identical (one outlier was excepted) among all NRs are shown in light green, those among NRs and animal SOs are shown in dark green, and those among the entire SO family of Mo enzymes (including both NRs and SOs) are shown in orange. Sequence alignments were generated with ClustalW, and the last residue of each sequence line is numbered. Surfaces were generated using GRASP (Nicholls et al., 1991) and rendered with POVRAY.

superimposing with their counterparts in PSO and CSO. Most importantly, Cys139 serving as third sulfur ligand of Mo is matching in all three enzymes (data not shown in Figure 5A) because it is the unique characteristic of enzymes of the SO family (Garrett and Rajagopalan, 1996; Garton et al., 1997; Su et al., 1997). On the other side, there are three residues, the strictly NR-conserved Asn272 and Met427, as well as the non-conserved Thr425 that seem to be unique in NR and probably crucial for nitrate binding and catalysis. For some of the corresponding residues, it has been shown in SO that they are important for catalysis. Asn272 is replaced by Tyr322 in CSO (Figure 5A), which is completely conserved among all known SOs and has been shown to be involved in intramolecular-coupled electron/proton transfer (Feng et al., 2003) as well as substrate binding and catalysis (Wilson and Rajagopalan, 2004).

In PSO and CSO, another residue (Arg374/Arg450) was suggested to be essential for substrate/product binding as indicated by a sulfate-dependent conformational change (Schrader et al., 2003). In this structure of *P. angusta* NR-Mo, this SO-conserved Arg is replaced by Thr425, which is not conserved among NRs. Fungal NRs either have a Thr or Leu, whereas in plant NRs, only Met is found at that position (Figure 1B). The third NR-specific and conserved active side residue is Met427 replacing a Val in SOs. Met cannot participate as electron donor in hydrogen bonds with its side chain, which is a main difference as compared with the SO-conserved Arg that might be able to form

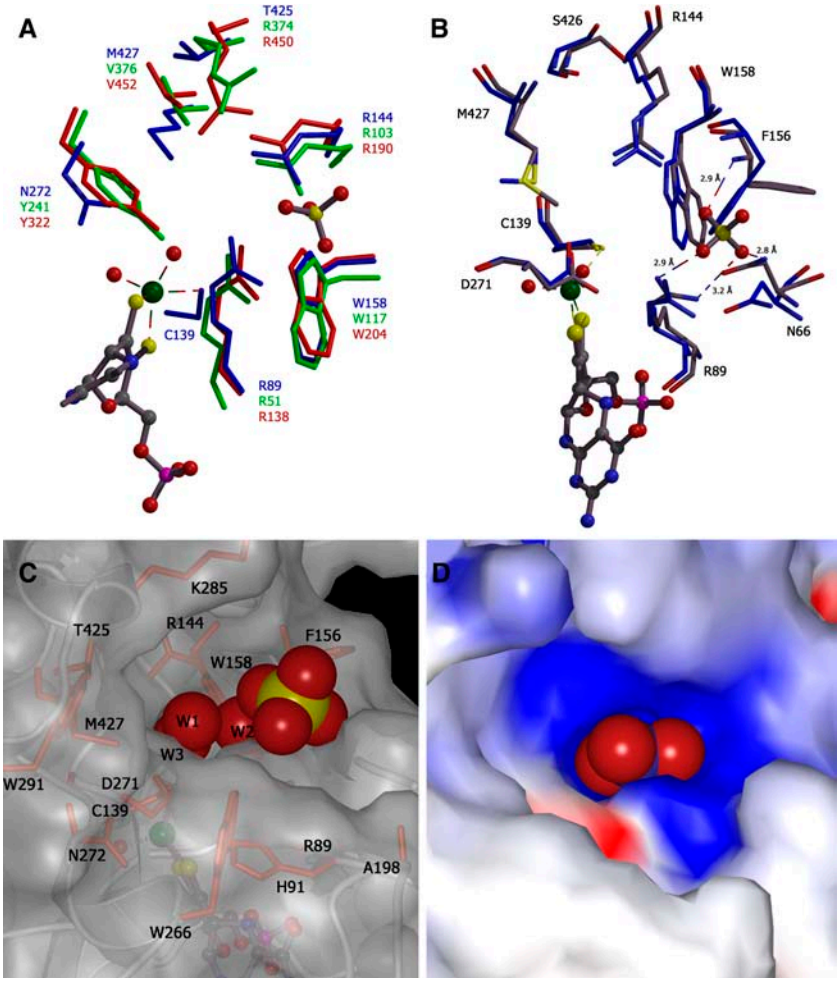

Figure 5. The Active Site of NR-Mo.

(A) Superposition of the active sites of NR-Mo2, PSO, and CSO. Residues of NR-Mo are color coded in blue, PSO in green, and CSO in red. All residues are shown in stick mode and are numbered in the corresponding color.
(B) Superposition of the active sites of NR-Mo1 (blue) and NR-Mo2 (gray). NR-Mo2 residues are colored in gray and NR-Mo1 in blue. In **(A)** and **(B)**, Moco (derived from NR-Mo2) and sulfate are shown in ball-and-stick mode, and both panels were generated with MOLSCRIPT (Esnouf, 1997).
(C) and **(D)** Surface representation of the substrate binding site of NR-Mo2 with the bound sulfate and three active site waters (W1-3) **(C)** and with nitrate superimposed onto the waters **(D)**; all are shown as a space-filling model. Surfaces are shown either transparent with highlighted and labeled active site residues or nontransparent and color coded according to the surface charge as shown in Figure 4A. The surfaces were made as described in Figure 4.

hydrogen bonds. Because of the distance of either Met427 in NR or Arg374 in PSO to the Mo center, a direct involvement in the reaction cycle of these residues is less possible. They seem to be either important as a general stabilizer of charges or they serve a steric function. This hypothesis is supported by the altered conformation of Met427 between the NR-Mo structures, which is reminiscent to the changes observed in SOs for Arg374/Arg450 (see below).

Bacterial dissimilatory NR forms contain a different molybdopterin-based cofactor, where Mo is coordinated by two molybdopterin dithiolates and each pterin is modified by a nucleotide attached via a pyrophosphate bond (Dobbek and Huber, 2002). Consequently, the overall fold of this class of enzymes is completely different from the fold of enzymes of the eukaryotic SO family (Dias et al., 1999). Despite the different fold, there are remarkable similarities. Both NR types have an additional sulfur ligand to Mo, which is derived from a conserved Cys. Furthermore, the same types of active site residues are conserved among dissimilatory NRs (Gln346, Arg356, and Met308 from *Desulfovibrio desulfuricans*) (Dias et al., 1999) and in *P. angusta* NR-Mo.

Sulfate-Induced Conformational Changes

In the high-resolution structure of NR-Mo2, one out of two sulfate molecules is well defined and in close proximity to the active site

(Figures 5A to 5C) next to the narrowing substrate entrance with an average distance of 8.8 Å to the Mo (Mo-S distance) in both monomers. This anion binding is accompanied by several conformational changes relative to NR-Mo1 with no sulfate bound. Changes appear close to the sulfate binding site and mainly affect active site residues (Figure 5B). Most remarkably, Phe156 shows a large rotation of the phenyl group in NR-Mo2. Two other residues, Asn66 and Arg89, together with Phe156 are directly involved in sulfate coordination. Several other active site residues, Arg144, Asp271, Trp158, and Ser426, are slightly distorted toward the bound sulfate. Finally, Met427, conserved in all NRs, occupies a conformation with its side chain pointing toward the Mo, whereas in NR-Mo1, the Met427 side chain turns away from the active site.

Because inorganic phosphate is known to be an activator of NR activity (Howard and Solomonson, 1981; Kay and Barber, 1989; Campbell, 2001), it is tempting to suggest that the sulfate binding site near the Mo could be the phosphate activator site of NR because sulfate is a structural mimic of phosphate. Thus, the conformational differences described above for NR-Mo2 might be related to those involved in NR activation by phosphate. Because crystallization experiments under similar conditions with phosphate failed to produce NR-Mo crystals, we cannot prove whether or not phosphate binds in a similar way to NR-Mo than sulfate. Kinetic studies on Chlorella NR have shown that sulfate can also activate NR but to a somewhat lesser extent than phosphate (Howard and Solomonson, 1981). It is important to note that this phosphate/sulfate-induced activation was only observed for the NADH-dependent NR activity but not for the NADH-dependent cytochrome *c* reductase activity. Already these findings strongly suggest that phosphate and sulfate act on the Mo domain of NR, which further strengthens our conclusions. Preliminary studies with *P. angusta* holo NR (data not shown) in the presence or absence of phosphate indicated no significant effect of sulfate on NR activity. Therefore, more detailed kinetic studies with holo-NR as well as NR-Mo are needed to investigate the functional role of both anions on the NR activity.

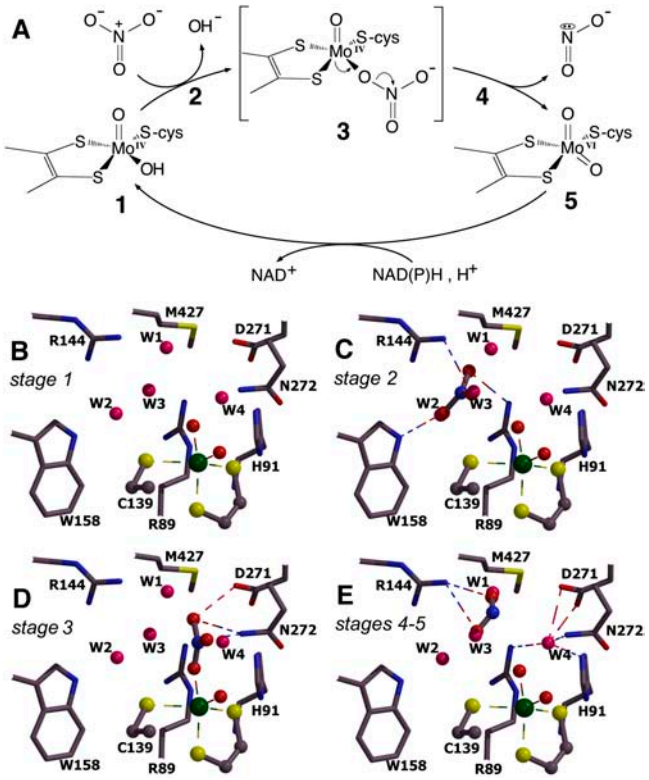

Figure 6. Hypothetical Reaction Cycle of Nitrate Reduction by NR.

(A) Reaction cycle of nitrate reduction by NR. The reaction starts with the reduced Mo(IV) center (stage 1). Nitrate binds to the active site (stage 2) and replaces the equatorial hydroxo/water ligand, thus forming the reaction intermediate (stage 3). Upon oxidation of the Mo center to Mo(VI), the bond between the nitrate oxygen and nitrogen is broken, and nitrite will be released (stages 4 and 5). After completion of the reductive half-reaction, the Mo is regenerated [Mo(IV)] for the next cycle.

(B) to **(E)** Models of the active site at different stages of the reaction cycle, generated with MOLSCRIPT and rendered with RASTER3D (Merritt and Murphy, 1994).

(B) View of the active site as seen in the 1.7-Å structure with four water molecules (W1 to W4) bound. The view resembles the situation shown in **(A)** at stage 1.

(C) Hypothetical binding of nitrate based on a superposition with W2 and W3 (stage 2 in **[A]**). The nitrate oxygen located at W3 attacks the Mo, and the Mo hydroxo ligand will be displaced to the position of W4.

(D) Formation of a penta-coordinated reaction intermediate with the nitrogen, nitrate-oxygen, Mo, and the apical oxygen forming a plane. The resulting hydrogen bonds of bound nitrate are indicated (stage 3 in **[A]**).

(E) The released nitrite is superimposed with W1 and W2 because of the high mobility of W1 (B-factor = 46).

The Nitrate Binding Site

In the active site of NR-Mo2, four ordered water molecules were identified that appear to mimic the binding site of nitrate (Figure 5C). Three of these water molecules are located in the core of the active site, and a nitrate molecule was superimposed onto two of these water molecules (W2 and W3), resulting in hydrogen bonds for all of the three nitrate oxygens to two active site Arg residues and one Trp (Figure 6C). All three residues involved in nitrate binding are conserved among all enzymes of the SO family, indicating a similar binding of nitrate and sulfite in NR and SO. One oxygen ($O3_{nitrate}$ lying on W3, B-factor = 28) points toward the equatorial hydroxo/water ligand of the Mo(IV) center with a distance of 2.8 Å and is hydrogen bonded to Arg144NH2. $O1_{nitrate}$ and $O2_{nitrate}$ (modeled onto W2, B-factor = 29) form hydrogen bonds to Arg89NH2 and Trp158NE1, respectively. In animal SO, it has been shown that the conserved Arg corresponding to Arg144 (Arg190 in CSO) is important for both substrate binding (Garrett et al., 1998) and intramolecular-coupled electron/proton transfer (Feng et al., 2003). Therefore, it is not surprising that Arg144 in NR coordinates the modeled nitrate molecule. So far, attempts to soak or cocrystallize NR-Mo with nitrate, nitrite, or both gave no sufficiently diffracting crystals. In the surface presentation of NR-Mo2, an elongated slot is formed at the entrance to the active site. Drawing a modeled nitrate molecule (Figure 5D) into a surface presentation as a space-filling model nicely illustrates

the almost perfect match between the surface depression and the shape of nitrate.

The Reaction Mechanism of Eukaryotic Nitrate Reduction

For nitrate reduction, NAD(P)H provides the FAD cofactor of NR with two electrons that are subsequently transferred via the cytochrome b_5 domain to the Moco that accomplishes the substrate reduction to nitrite. Based on reaction kinetic studies (Skipper et al., 2001), the functional similarity to SOs (Kisker et al., 1997) and the presented crystal structures of NR-Mo, we describe a general model for the reaction mechanism of nitrate reduction in eukaryotic NRs (Figure 6A). We took advantage of three highly ordered water molecules and one moderately ordered water molecule (Figure 6B) to propose the binding of nitrate (Figure 6C), the formation of a penta-coordinated reaction intermediate (Figure 6D), and the release of the products nitrite and water (Figure 6E).

In our reaction model, first the substrate nitrate binds to the reduced Mo(IV) form as shown in Figure 6C. Upon nitrate binding, the oxygen (corresponding to W3, Figure 6B) closest to Mo attacks the metal center, thereby displacing the equatorial hydroxo/water ligand (O6) from Mo, thus forming the reaction intermediate (Figure 6D). The displaced hydroxo/water ligand might occupy the position of the water W4 (Figure 6E), which is coordinated by Asp271, Asn272, Arg89, and His91. Three of these residues (Asp271, Arg89, and His91) are completely conserved throughout the entire SO family, possibly indicating a conserved mechanism for the oxo-transfer reaction catalyzed by NR and SO. The position of the reaction intermediate (Figure 6D) was chosen by a planarity restrain for the nitrogen, nitrate-oxygen, Mo, and the apical oxygen bonds according to the stereochemistry and reaction of model compounds (Pietsch and Hall, 1996), and reasonable distances to adjacent atoms were also considered. The resulting coordination of the bound nitrate involves Asp271 and Asn272. When superimposing this reaction intermediate onto the NR-Mo1 structure, Met427 might form an additional contact to the reaction intermediate (data not shown), indicating a functional importance of this residue during catalysis. Asn272 and Met427 are exclusively conserved in NRs and are therefore crucial for catalysis because they participate in the coordination of both the leaving hydroxo/water ligand and the reaction intermediate (Figures 6D and 6E). Once the reaction intermediate is formed, the electrons of the Mo d-orbital flip over to the Mo-$O_{nitrate}$ bond, thereby forming the second Mo-O bond and causing the oxidation of Mo(IV) to Mo(VI) (Figure 6A). The latter is accompanied by the release of nitrite, which might be coordinated by Arg144, a residue conserved in the entire SO family (Figure 6E). Upon product formation, the Mo center can be regenerated by the reductive half reaction, where two electrons derived from NAD(P)H are transferred via an intramolecular electron transport chain to the Mo.

For NR, product inhibition by nitrite is known with a K_i = 330 μM for Chlorella NR, whereas the K_m for nitrate is ~30 μM (Howard and Solomonson, 1981). The proposed coordination of nitrate by three hydrogen bonds is in agreement with the K_m value for nitrate. Furthermore, the coordination of nitrite by two hydrogen bonds, derived from the substrate binding Arg144, explains the observed nitrite product inhibition with a K_i 10 times higher than the K_m for nitrate, which is related to the loss of one hydrogen bond during product binding.

In our model, Asp271 and Asn272 play a crucial role for displacing the Mo-hydroxo/water ligand, as well as stabilizing the reaction intermediate. In addition to the proposed interactions, Asn272 appears to be well positioned (Asn272δN-MocoO6 distance of 3.3 to 3.6 Å) to participate in catalysis because the neighboring Asp271 might be able to exhibit an electronegative force onto the Asp carbamide group. In contrast with the strictly conserved Tyr in SO (Tyr241/Tyr322), Asn272 is not capable to act as a proton shuttle, but as a potent stabilizer for either cations or anions.

For dissimilatory NR, a model with a similar reaction intermediate has been proposed (Dias et al., 1999). Despite the above-mentioned differences between eukaryotic and bacterial NR, the presence of similar and conserved active site residues in both Mo enzymes might suggest a common and conserved reaction chemistry for the reduction of nitrate by mononuclear Mo centers, and it could reflect the evolutionary pressure to maintain a unique Mo center for nitrate reduction. In particular, the presence of a conserved Glu in bacterial NR (Dias et al., 1999) and the conserved Asp in NR-Mo in close proximity to the Mo supports the functional importance of the amide group in both Mo-dependent NRs.

In summary, the structure of NR-Mo confirmed the overall similarity of NR and SO, both on structural and functional levels. Regarding the similar size and type of both nitrate and sulfite, substrate binding is proposed to be very similar due to three overall conserved residues. However, the formation of the reaction intermediate as well as product release is tightly associated with NR-specific residues. Consequently, the question might be raised whether or not it is possible to convert the nitrate-reducing Mo fragment into an oxidase or vice versa. Therefore, the structure-based model for the reaction mechanism of NR provides a unique framework for future structure–function studies of eukaryotic NRs.

METHODS

Protein Expression and Purification

NR-Mo was derived from *Pichia angusta* YNR1. YNR1 was cloned with a methanol-induced promoter in pPICZ-B plasmid (Invitrogen, Carlsbad, CA) and modified by site-directed mutagenesis to introduce a hexaHis-tag at the N-terminal part of the protein and a stop codon in the hinge 1 part of the protein. Approximayely 1 μg of linearized plasmid was used to transform electrocompetent wild-type *P. pastoris* by electroporation. After NR-Mo expressing cell line selection, fermentation was performed as described for the related fragment of YNR1, which is called simplified NR or S-NaR1 (Barbier et al., 2004). The disruption of the cells and the purification of the crude NR-Mo by immobilized metal affinity chromatography were done according to the protocol previously described for S-NaR1. At this stage, the NR-Mo fragment catalyzed production of nitrite from nitrate with a $k_{cat} = 160\ s^{-1}$ using dithionite-reduced methyl viologen as electron donor, which is similar to the catalytic turnover of nitrate reduction catalyzed by holo-NR (Campbell, 2001; Skipper et al., 2001). NR-Mo was buffer-exchanged by dialysis into 50 mM Tris, pH 7.5, 50 mM NaCl, and 2 mM DTT. NR-Mo was further enriched by anion-exchange

chromatography on a 10-mL SourceQ15 column (Amersham-Pharmacia Biotech, Uppsala, Sweden) with the protein eluting at 250 mM NaCl. After concentrating the protein, preparative size exclusion chromatography (Superose 26/60; Amersham-Pharmacia Biotech) was performed with a buffer containing 50 mM Tris, pH 7.5, 200 mM NaCl, 1 mM EDTA, and 2 mM DTT. A single peak corresponding to the size of the NR-Mo dimer was obtained. The protein buffer was exchanged to the crystallization buffer (20 mM Tris, pH 7.5, 50 mM NaCl, and 5 mM DTT), and the protein was concentrated to 12 mg/mL and stored in aliquots at −80°C after flash freezing in liquid nitrogen.

Crystallization and Structure Determination of NR-Mo1

The NR-Mo1 crystal type grew at 23°C by vapor diffusion against a reservoir of solution 7 from the Hampton Crystal Screen II (Hampton Research, Aliso Viejo, CA) within 1 d. These crystals diffracted x-rays to 2.6 Å resolution using synchrotron radiation of beamline BW6 at the Deutsches Elektronensynchrotron (DESY) (Hamburg, Germany), and a data set was collected using a MAR CCD detector (Marresearch, Norderstedt, Germany). Data were indexed, integrated, and scaled with the HKL-suite (Otwinowski and Minor, 1997), and all subsequent calculations were performed with the CCP4 suite (Collaborative Computational Project Number 4, 1994) with exceptions as indicated.

Based on the unit cell dimensions (Table 1) of the hexagonal crystal with space group $P6_122$, one monomer per asymmetric unit was predicted, yielding a Matthew's coefficient of 2.3 $Å^3$/D and 47.1% solvent content. The structure was solved by molecular replacement with AMORE (Navaza, 1994) using a monomer of PSO (Schrader et al., 2003) as search model. The quality of the obtained solution was evaluated by the crystallographically related objects that should form a dimer similar to PSO and CSO. Refinement was performed with REFMAC5 (Murshudov et al., 1997) followed by manual rebuilding of the structure in O (Jones et al., 1991). Water molecules were included using ARP_WARP (Perrakis et al., 2001).

Crystallization and Structure Determination of NR-Mo2

Initial NR-Mo microcrystals of another type were obtained after ~2 weeks with solution 26 from Hampton Crystal Screen II (Hampton Research). The refinement of the crystallization condition led to one single crystal growing after 10 weeks in a solution containing 24% PEG MME 5000 (Fluka, Buchs, Switzerland), 0.1 M Mes, pH 6.5, and 0.3 M ammonium sulfate. This orthorhombic crystal diffracted to a resolution of 1.7 Å, and a data set was recorded at beamline BW6 at DESY (Hamburg, Germany). With the unit cell dimensions and the noncrystallographic symmetry operations, the asymmetric unit of this $C222_1$ crystal was calculated to comprise two monomers, resulting in a Matthew's coefficient of 2.9 $Å^3$/D and 57.3% solvent content. Integration was executed with MOSFLM (Leslie, 1992), and scaling and further calculations were conducted with programs form the CCP4 suite. Initial phasing attempts by molecular replacement with PSO or CSO as search models using AMORE or MOLREP (Vagin and Teplyakov, 1998) failed, but finally succeeded using the refined NRMo1 structure. Both monomers formed crystallographic dimers.

Atomic coordinates and structure factors of NR-Mo1 (2BIH) and NR-Mo2 (2BII) have been deposited in the Research Collaboratory for Structural Bioinformatics Protein Data Bank.

ACKNOWLEDGMENTS

We thank Russ Hille (Ohio State University, Columbus, OH) and Caroline Kisker (State University of New York, Stony Brook, NY) for helpful discussions and critical reading of the manuscript. Special thanks to Nils Schrader (Technical University of Braunschweig, Germany) for great company and help throughout the entire project. This work was supported by Deutsche Forschungsgemeinschaft Grant Schw759/3-1 (G.S.) and by a National Institutes of Health Small Business Innovation Research grant to the Nitrate Elimination Company (contract R44GM56598). We gratefully acknowledge the support by the staff at Beamline BW6 at DESY (Hamburg, Germany) and at Protein Structure Factory Beamline 1 at Berliner Elektronenspeicherring-Gesellschaft für Synchrotronstrahlung (Berlin, Germany).

Received November 24, 2004; accepted February 3, 2005.

REFERENCES

Bahadur, R.P., Chakrabarti, P., Rodier, F., and Janin, J. (2004). A dissection of specific and non-specific protein-protein interfaces. J. Mol. Biol. **336,** 943–955.

Barbier, G.G., Joshi, R.C., Campbell, E.R., and Campbell, W.H. (2004). Purification and biochemical characterization of simplified eukaryotic nitrate reductase expressed in *Pichia pastoris*. Protein Expr. Purif. **37,** 61–71.

Barton, G.J. (1993). ALSCRIPT: A tool to format multiple sequence alignments. Protein Eng. **6,** 37–40.

Campbell, W.H. (2001). Structure and function of eukaryotic NAD(P)H: nitrate reductase. Cell. Mol. Life Sci. **58,** 194–204.

Campbell, W.H., and Kinghorn, K.R. (1990). Functional domains of assimilatory nitrate reductases and nitrite reductases. Trends Biochem. Sci. **15,** 315–319.

Collaborative Computational Project, Number 4 (1994). The CCP4 suite: Programs for protein crystallography. Acta Crystallogr. D Biol. Crystallogr. **50,** 760–763.

Combet, C., Blanchet, C., Geourjon, C., and Deleage, G. (2000). NPS@: Network protein sequence analysis. Trends Biochem. Sci. **25,** 147–150.

Dias, J.M., et al. (1999). Crystal structure of the first dissimilatory nitrate reductase at 1.9 Å solved by MAD methods. Structure **7,** 65–79.

Dobbek, H., and Huber, R. (2002). The molybdenum and tungsten cofactors: A crystallographic view. Met. Ions Biol. Syst. **39,** 227–263.

Eilers, T., Schwarz, G., Brinkmann, H., Witt, C., Richter, T., Nieder, J., Koch, B., Hille, R., Hansch, R., and Mendel, R.R. (2001). Identification and biochemical characterization of *Arabidopsis thaliana* sulfite oxidase. A new player in plant sulfur metabolism. J. Biol. Chem. **276,** 46989–46994.

Esnouf, R.M. (1997). An extensively modified version of MolScript that includes greatly enhanced coloring capabilities. J. Mol. Graph. Model. **15,** 132–134, 112–113.

Feng, C., Kedia, R.V., Hazzard, J.T., Hurley, J.K., Tollin, G., and Enemark, J.H. (2002). Effect of solution viscosity on intramolecular electron transfer in sulfite oxidase. Biochemistry **41,** 5816–5821.

Feng, C., Wilson, H.L., Hurley, J.K., Hazzard, J.T., Tollin, G., Rajagopalan, K.V., and Enemark, J.H. (2003). Role of conserved tyrosine 343 in intramolecular electron transfer in human sulfite oxidase. J. Biol. Chem. **278,** 2913–2920.

Garrett, R.M., Johnson, J.L., Graf, T.N., Feigenbaum, A., and Rajagopalan, K.V. (1998). Human sulfite oxidase R160Q: Identification of the mutation in a sulfite oxidase-deficient patient and expression and characterization of the mutant enzyme. Proc. Natl. Acad. Sci. USA **95,** 6394–6398.

Garrett, R.M., and Rajagopalan, K.V. (1996). Site-directed mutagenesis of recombinant sulfite oxidase: Identification of cysteine 207 as a ligand of molybdenum. J. Biol. Chem. **271,** 7387–7391.

Garton, S.D., Garrett, R.M., Rajagopalan, K.V., and Johnson, M.K. (1997). Resonance raman characterization of the molybdenum center

in sulfite oxidase: Identification of Mo=O stretching modes. J. Am. Chem. Soc. **119,** 2590–2591.

George, G.N., Pickering, I.J., and Kisker, C. (1999). X-ray absorption spectroscopy of chicken sulfite oxidase crystals. Inorg. Chem. **38,** 2539–2540.

Hille, R. (1996). The mononuclear molybdenum enzymes. Chem. Rev. **96,** 2757–2816.

Howard, W.D., and Solomonson, L.P. (1981). Kinetic mechanism of assimilatory NADH:nitrate reductase from Chlorella. J. Biol. Chem. **256,** 12725–12730.

Hutchinson, E.G., and Thornton, J.M. (1996). PROMOTIF–A program to identify and analyze structural motifs in proteins. Protein Sci. **5,** 212–220.

Jones, T.A., Zou, J.Y., Cowan, S.W., and Kjeldgaard, M. (1991). Improved methods for building protein models in electron density maps and the location of errors in these models. Acta Crystallogr. A **47,** 110–119.

Kaiser, W.M., and Huber, S.C. (2001). Post-translational regulation of nitrate reductase: Mechanism, physiological relevance and environmental triggers. J. Exp. Bot. **52,** 1981–1989.

Kay, C.J., and Barber, M.J. (1989). EPR and kinetic analysis of the interaction of halides and phosphate with nitrate reductase. Biochemistry **28,** 5750–5758.

Kessler, D.L., and Rajagopalan, K.V. (1974). Hepatic sulfite oxidase. Effect of anions on interaction with cytochrome c. Biochim. Biophys. Acta **370,** 389–398.

Kisker, C., Schindelin, H., Pacheco, A., Wehbi, W.A., Garrett, R.M., Rajagopalan, K.V., Enemark, J.H., and Rees, D.C. (1997). Molecular basis of sulfite oxidase deficiency from the structure of sulfite oxidase. Cell **91,** 973–983.

Laskowski, R.A., Moss, D.S., and Thornton, J.M. (1993). Main-chain bond lengths and bond angles in protein structures. J. Mol. Biol. **231,** 1049–1067.

Leslie, A.G.W. (1992). Recent changes to the MOSFLM package for processing film and image plate data. Joint CCP4 + ESF-EAMCB Newsletter on Protein Crystallography, No. 26.

Lu, G., Campbell, W., Lindqvist, Y., and Schneider, G. (1992). Crystallization and preliminary crystallographic studies of the FAD domain of corn NADH:nitrate reductase. J. Mol. Biol. **224,** 277–279.

Lu, G., Campbell, W.H., Schneider, G., and Lindqvist, Y. (1994). Crystal structure of the FAD-containing fragment of corn nitrate reductase at 2.5 A resolution: Relationship to other flavoprotein reductases. Structure **2,** 809–821.

Lu, G., Lindqvist, Y., Schneider, G., Dwivedi, U., and Campbell, W. (1995). Structural studies on corn nitrate reductase: Refined structure of the cytochrome b reductase fragment at 2.5 A, its ADP complex and an active- site mutant and modeling of the cytochrome b domain. J. Mol. Biol. **248,** 931–948.

MacKintosh, C., and Meek, S.E. (2001). Regulation of plant NR activity by reversible phosphorylation, 14-3-3 proteins and proteolysis. Cell. Mol. Life Sci. **58,** 205–214.

Mendel, R.R., and Schwarz, G. (1999). Molybdoenzymes and molybdenum cofactor in plants. Crit. Rev. Plant Sci. **18,** 33–69.

Merritt, E.A., and Murphy, M.E.P. (1994). Raster3D Version 2.0. A program for photorealistic molecular graphics. Acta Crystallogr. D Biol. Crystallogr. **50,** 869–873.

Murshudov, G., Vagin, A., and Dodson, E. (1997). Refinement of macromolecular structures by the maximum-likelihood method. Acta Crystallogr. D Biol. Crystallogr. **53,** 240–255.

Navaza, J. (1994). AMORE: An automated package for molecular replacement. Acta Crystallogr. A **50,** 157–163.

Nicholls, A., Sharp, K.A., and Honig, B. (1991). Protein folding and association: Insights from the interfacial and thermodynamic properties of hydrocarbons. Proteins **11,** 281–296.

Nussaume, L., Vincentz, M., Meyer, C., Boutin, J.P., and Caboche, M. (1995). Post-transcriptional regulation of nitrate reductase by light is abolished by an N-terminal deletion. Plant Cell **7,** 611–621.

Otwinowski, Z., and Minor, W. (1997). Processing of X-ray diffraction data collected in oscillation mode. In Methods in Enzymology: Macromolecular Crystallography, C.W. Carter and R.M. Sweet, eds (San Diego: Academic Press), pp. 307–326.

Perrakis, A., Harkiolaki, M., Wilson, K.S., and Lamzin, V.S. (2001). ARP/wARP and molecular replacement. Acta Crystallogr. D Biol. Crystallogr. **57,** 1445–1450.

Pietsch, M.A., and Hall, M.B. (1996). Theoretical studies on models for the oxo-transfer reaction of dioxomolybdenum enzymes. Inorg. Chem. **35,** 1273–1278.

Pollock, V.V., Conover, R.C., Johnson, M.K., and Barber, M.J. (2002). Bacterial expression of the molybdenum domain of assimilatory nitrate reductase: Production of both the functional molybdenum-containing domain and the nonfunctional tungsten analog. Arch. Biochem. Biophys. **403,** 237–248.

Ratnam, K., Shiraishi, N., Campbell, W.H., and Hille, R. (1997). Spectroscopic and kinetic characterization of the recombinant cytochrome c reductase fragment of nitrate reductase. Identification of the rate-limiting catalytic step. J. Biol. Chem. **272,** 2122–2128.

Schrader, N., Fischer, K., Theis, K., Mendel, R.R., Schwarz, G., and Kisker, C. (2003). The crystal structure of plant sulfite oxidase provides insights into sulfite oxidation in plants and animals. Structure **11**, 1251–1263.

Skipper, L., Campbell, W.H., Mertens, J.A., and Lowe, D.J. (2001). Pre-steady-state kinetic analysis of recombinant Arabidopsis NADH: nitrate reductase: Rate-limiting processes in catalysis. J. Biol. Chem. **276,** 26995–27002.

Stolz, J.F., and Basu, P. (2002). Evolution of nitrate reductase: Molecular and structural variations on a common function. Chembiochem **3,** 198–206.

Su, W., Mertens, J.A., Kanamaru, K., Campbell, W.H., and Crawford, N.M. (1997). Analysis of wild-type and mutant plant nitrate reductase expressed in the methylotrophic yeast *Pichia pastoris*. Plant Physiol. **115,** 1135–1143.

Thompson, J.D., Higgins, D.G., and Gibson, T.J. (1994). CLUSTAL W: Improving the sensitivity of progressive multiple sequence alignment through sequence weighting, position-specific gap penalties and weight matrix choice. Nucleic Acids Res. **22,** 4673–4680.

Vagin, A., and Teplyakov, A. (1998). A translation-function approach for heavy-atom location in macromolecular crystallography. Acta Crystallogr. D Biol. Crystallogr. **54,** 400–402.

Vaughn, D.E., and Bjorkman, P.J. (1996). The (Greek) key to structures of neural adhesion molecules. Neuron **16,** 261–273.

Wallace, A.C., Laskowski, R.A., and Thornton, J.M. (1995). LIGPLOT: A program to generate schematic diagrams of protein-ligand interactions. Protein Eng. **8,** 127–134.

Wilson, H.L., and Rajagopalan, K.V. (2004). The role of tyrosine 343 in substrate binding and catalysis by human sulfite oxidase. J. Biol. Chem. **279,** 15105–15113.